THE ASTROPHYSICAL JOURNAL, 211:91–107, 1977 January 1

THE RATIO OF DEUTERIUM TO HYDROGEN IN INTERSTELLAR SPACE. III. THE LINES OF SIGHT TO ZETA PUPPIS AND GAMMA CASSIOPEIAE

A. VIDAL-MADJAR,* C. LAURENT, AND R. M. BONNET
Laboratoire de Physique Stellaire et Planetaire,
Centre National de la Recherche Scientifique,
Verrieres-le-Buisson, France

AND

DONALD G. YORK
Princeton University Observatory
Received 1976 February 27; revised 1976 June 22

ABSTRACT

An extensive set of measurements of the ratio of deuterium to hydrogen in the interstellar medium has been undertaken. In this paper, we describe the general observing program, the data reduction techniques used to separate the complex deuterium and hydrogen profiles, and the results of the measurements for two stars: ζ Pup and γ Cas.

We find, for γ Cas, $\log N(\mathrm{D})/N(\mathrm{H}) = -4.8 \pm 0.1$, in agreement with previous measurements. For ζ Pup a complicated structure of absorbing clouds in the interstellar medium is inferred. The best value is about $\log N(\mathrm{D})/N(\mathrm{H}) = -4.6$ for each of two components. One component is probably more complex than can be demonstrated directly at our resolution, and $\log N(\mathrm{D})/N(\mathrm{H})$ could be -4.0 or larger in this component.

Subject headings: interstellar: abundances — interstellar: matter

I. INTRODUCTION

The determination of the ratio of deuterium to hydrogen has been successfully accomplished in several sources recently, including the solar corona (Hall 1974, unpublished; Anglin, Dietrich, and Simpson 1973), Jupiter (Beer and Taylor 1973; Trauger *et al.* 1973), molecular clouds in interstellar space (Wilson, Penzias, and Jefferts 1973) and diffuse interstellar space (Spitzer *et al.* 1973; Rogerson and York 1973 [Paper I of this series]; York and Rogerson 1976 [Paper II]). The D/H ratio thus determined applied to D and H in combination with other elements, not to D and H in atomic form, except for Papers I and II. Upper limits have been set for the Sun based on solar wind data (Geiss and Reeves 1972) and from meteoritic data (Black 1972), as well as from very long path lengths in interstellar space (Cesarsky, Moffet, and Pasachoff 1973; Pasachoff and Cesarsky 1974).

The presently available results show that $N(\mathrm{D})/N(\mathrm{H})$ in interstellar space, now and at the time of formation of the Sun, is about $(2 \pm 1) \times 10^{-5}$. The mass fraction of deuterium which follows from this measurement can be used to determine, formally at least, the present density of the Universe, if one adopts the view that deuterium has been formed during the primeval phases of the Universe (Wagoner 1973; Reeves *et al.* 1973). The actual formal density depends on the assumed values of the muon and electron lepton numbers (Yahil and Beaudet 1976); but if these numbers are zero, as is commonly assumed, the deuterium values quoted imply a mean density so low that the universe is not bound.

One important point to establish is the true site of formation of the deuterium. Observationally, one can ask just how variable the ratio $N(\mathrm{D})/N(\mathrm{H})$ actually is within our own Galaxy. If the deuterium is primordial, one expects some local deviation in the sense that D must be lower in regions where active star formation occurs, because stars consume deuterium but do not expel any to interstellar gas, because of the efficiency of nuclear reactions destroying it.

On the other hand, if deuterium is formed locally, for instance by supernovae (Colgate 1975), a reverse correlation must be found as suggested by Ostriker and Tinsley (1975). The question of the point-to-point contrast has not been explored in the literature. In the case of variations due to astration, since this process works for nearly all stars, local variations are probably smoothed by looking over lines of sight of 100 pc, which contain several regions of star formation. For local production mechanisms, there will be some dilution as the expanding region around the supernova sweeps up interstellar matter. Both processes are affected by the fact that mixing in the interstellar gas could be efficient in lowering any contrast produced, especially if the bulk of star formation and

* Guest Investigator with the Princeton University telescope on the *Copernicus* satellite, which is sponsored and operated by the National Aeronautics and Space Administration.

destruction occurred early in the evolution of the Galaxy as suggested by most of the present models of chemical evolution (Truran and Cameron 1971; Talbot and Arnett 1973; Quirk and Tinsley 1973; Audouze and Tinsley 1974).

Nevertheless, the data from the *Copernicus* instrument will soon lead to the availability of relative abundances for many elements over a wide range of lines of sight so that at least a differential comparison of the variability of various abundance ratios to that of $N(\mathrm{D})/N(\mathrm{H})$ can be made.

We have therefore undertaken a program of detection of interstellar deuterium in lines of sight which extend beyond the stars which lie within 200 pc of the Sun. In making this extension, one is faced with several difficulties described in § II. The techniques used in deriving the deuterium for each interstellar component are described in § III, which includes an analysis of errors in measurement. The results are summarized in § IV.

II. OBSERVING PROGRAM

The observational limitations of the proposed program are: (1) the need to observe absorption lines in spectra of stars with $v \sin i \geq 50$ km s^{-1}, since the *Copernicus* resolution is about 15 km s^{-1}; (2) the reduction in signal at deuterium and hydrogen wavelengths caused by coincident lines of interstellar molecular hydrogen and by stellar hydrogen absorption; (3) the reduction in signal due to low mirror reflectivity (system efficiency $\sim 0.03\%$ at 950 Å) and the rapidly rising UV extinction in interstellar clouds (York *et al.* 1973); and (4) the increase in number of interstellar components with distance, which tends, at our resolution, to smear out separate components and compromise the accuracy of the analysis.

The problem of overall efficiency restricts us to studying stars brighter than fourth magnitude in a survey such as this. Stellar hydrogen lines are shallow enough to allow observations for stars earlier than B1. The problems of extinction and of coincident H_2 lines limit useful observations to stars with $E(B - V) \leq 0.1$. Choosing only simple lines of sight is difficult, *a priori*, because the most useful observations in this regard are of Na I and Ca II lines (Hobbs 1969; Marschall and Hobbs 1972), whose column density depends on $N(\mathrm{Na})$ or $N(\mathrm{Ca})$, and n_e, whereas $N(\mathrm{D\ I})$ is independent of n_e. Hence, we have essentially used the restriction of magnitude and extinction in choosing stars. We have maintained the requirement of being able to observe at least three deuterium lines to allow internal consistency checks on the accuracy of the derived abundances.

There are about 20 stars which are useful, of which β Cen, α Cru, α Vir, γ^2 Vel, and μ Col have been previously observed (Paper II). For this more extensive program we have chosen to scan the deuterium and hydrogen resonance lines Lβ, Lγ, Lδ, and Lϵ, using tube U1 (Rogerson, Spitzer, *et al.* 1973). In addition, a wide enough wavelength range was included in each scan to obtain a few other interstellar lines (chiefly O I and H_2), as well as some indication of the shape of the stellar spectrum, needed for accurately defining the continuum.

III. DATA PROCESSING

Previous abundance determinations have been done through the use of the curve-of-growth technique, which has the very important advantage of giving a result independent of the instrumental profile used for the observation. Nevertheless, it is well known, as demonstrated by different authors (Nachman and Hobbs 1973; Gomez-Gonzalez and Lequeux 1975), that this technique may induce large errors, particularly in the flat portion of the curve of growth, essentially because the absorbers are not in a single simple cloud but in several clouds having different velocities corresponding to different and overlapping Doppler shifts.

To partially overcome this difficulty, we have tried to use the information included in the line profiles to separate the cloud components. A deconvolution of the observed spectra was performed by introducing in the calculations the instrumental profile of the Princeton instrument. Because the studied cases represent solutions spread over the full curve of growth (hydrogen and deuterium observed in four different Lyman lines), we had to make precise calculations using a full Voigt profile calculation (Morton and Morton 1972). Two of us (A. V.-M. and C. L.) prepared model fitting programs following Kaper *et al.* (1966), giving the possibility of separating up to seven cloud components along a given line of sight.

a) The Data Processing Principles

1. Because the Princeton instrument has a very narrow entrance slit (0.″3), the slightest pointing motion induces flux variations which introduce a nonrandom noise over the data. To correct this effect, it was only necessary to use the data collected with another channel (U2) fixed in wavelength while the stellar spectrum was measured through the U1 channel (short wavelength range and high resolution; see Rogerson, Spitzer, *et al.* 1973). The data introduced in all calculations were then corrected through the following relation:

$$U = \frac{U_1}{U_2} \cdot \overline{U}_2 , \qquad (1)$$

where $\overline{U}_2$ represents the average value of all the counts collected by the U2 channel during the completion of one given spectrum. As the nonrandom fluctuations may approach 10% in our data sample, the resulting improvement in the data quality is quite important.

2. The general equations used to fit the data represent classical line profile calculations using simultaneously the Doppler core and the damping wing formulation through the Harris function noted here as $H(a, w)$. Under such conditions the absorption

introduced into a stellar spectrum at a given wavelength λ may be represented by the following function:

$$A(\lambda) = \exp\left[-\sum_{i=1}^{n} k_0{}^i H(a^i, w^i) N^i\right] = A(\lambda, N^i, T^i, v^i), \quad (2)$$

where n is the number of clouds (up to seven) and i is a superscript representing one of the absorbing clouds, $k_0{}^i$ the absorption coefficient per absorber at line center, N^i the cloud column density, T^i the cloud temperature related to the classical b-value by $b^i = (2kT^i/m)^{1/2}$, and v^i the global velocity of the cloud relative to the star. Since we will analyze in general small spectral ranges over the spectra of fast rotating stars, the stellar spectrum $F_S(\lambda)$ may be approximated in such regions quite well by a parabola $F_S(\lambda, \alpha, \beta, \gamma)$ (three parameters as shown in the different figures presenting the data).

Finally, to represent the measurements $U(\lambda_m)$ taken at the wavelength λ_m we have to calculate the convolution of the spectrum by the instrumental profile which was assumed as a triangle of half width λ_p:

$$I(\lambda, \lambda_p, \lambda_m) = \frac{1}{\lambda_p}\left(1 \pm \frac{\lambda - \lambda_m}{\lambda_p}\right), \quad (3)$$

where the sign is positive for $\lambda_m - \lambda_p < \lambda < \lambda_m$ and negative for $\lambda_m < \lambda < \lambda_p + \lambda_m$. $I(\lambda, \lambda_p, \lambda_m) = 0$ for $\lambda < \lambda_m - \lambda_p$ or $\lambda > \lambda_p + \lambda_m$. Then the measurements should be compared with the following numerical evaluation:

$$U(\lambda_m) = B + \int_{\lambda_m - \lambda_p}^{\lambda_m + \lambda_p} F_S(\lambda, \alpha, \beta, \gamma) A(\lambda, N^i, T^i, v^i) \times I(\lambda, \lambda_p, \lambda_m)\, d\lambda, \quad (4)$$

where B represents the background.

To fit this theoretical evaluation to the data, we used an iterative process similar to the one described by Kaper *et al.* (1966) which allowed us to find the best parameters.

3. The instrumental profile width, λ_p, was evaluated using unsaturated absorption lines due to molecular hydrogen (at 1024.366 Å, for instance) in the spectrum of a bright star, γ Cas, or the deuterium lines themselves in the spectrum of γ Cas and ζ Pup.

The results obtained show that the best fits are generally obtained with λ_p values larger than 0.04 Å and less than 0.05 Å, the values for which the sum of the squares of the differences starts to rise significantly. Furthermore, as will be shown in the ζ Pup study, a lower value of λ_p seems to be preferred to a higher one.

Under such conditions all the following calculations were done with a λ_p value of 0.045 Å (but see Spitzer and Morton 1976) for all studied wavelengths, the effect of changing λ_p being studied only in one particular case (γ Cas).

b) Data Processing Method

To analyze the data, we will now have to pass through three different steps which will give us successively: the shape of the shortward wing of the hydrogen absorption line where the deuterium absorption takes place (phase I); the deuterium cloud parameters (phase II); the whole absorption profile due to hydrogen since it is necessary to evaluate also hydrogen column densities to deduce the relative deuterium abundances (phase III).

i) *Phase I*

Introducing into the calculations a few data points on either side of the deuterium absorption feature (not including the points of the absorption feature itself), and solving equation (4) for one hydrogen cloud, we end with a set of parameters: B, α, β, γ, N^H, T^H, v^H, λ_p, which have no real physical meaning but are necessary to represent the hydrogen absorption shortward wing. These parameters will then be used as input data in the next phase.

ii) *Phase II*

To evaluate now the parameters of the deuterium absorbing cloud, we may write equation (4) in the following form:

$$U(\lambda_m) = B + \int_{\lambda_m - \lambda_p}^{\lambda_m + \lambda_p} F_S(\lambda, \alpha, \beta, \gamma) \times A(\lambda, N^H, T^H, v^H) A(\lambda, N^i, T^i, v^i) I(\lambda, \lambda_p, \lambda_m)\, d\lambda, \quad (5)$$

where the only parameters are N^i, T^i, and v^i as the other values are taken from phase I. To find the solution, we have to operate step by step, finding first a single deuterium cloud that fits the data. Then by looking at the differences between $U(\lambda_m)$ and the observations it is easy to deduce the existence of other weaker clouds around the main one. Furthermore, with such a formulation, it is also possible to see how much matter may be hidden without disturbing the fit, giving a more precise evaluation of the error bars, as will be shown for specific cases.

iii) *Phase III*

Using now phase II results, some physical parameters, T^i or b^i and v^i of the main absorbing clouds, it is possible to introduce this information in a calculation which will try to represent the whole absorption line.

Under such conditions, through the use of equation (4) we evaluate the parameters α, β, γ, representing a broad parabolic variation, and N^i, the unknown column densities.

One may criticize each part of each phase described above independently; but because we have three or four different lines for each star to study and because hydrogen and deuterium should have the same physical parameters in the various velocity components observed, it is possible for us in such a study to iterate between phase II and phase III as well as between one Lyman line and another. The results, consistent over eight independent sets of observations (two absorbing species in four different lines),

present then a much higher degree of confidence, as will be shown now for γ Cas and ζ Pup.

For general reference, we list in Table 1 the interstellar features likely to occur in studies of deuterium.

IV. RESULTS AND DISCUSSION

a) γ *Cassiopeiae*

All the data collected on the four studied Lyman lines along with other interstellar absorption features, mainly due to molecular hydrogen or atomic oxygen, are shown in Figure 1. Detected interstellar lines are labeled. Table 1 includes a complete list of interstellar lines, with f-values, which might occur in the wavelength regions plotted. The search for the one cloud solution on the less saturated deuterium lines (Lδ and Lϵ) is presented on Figure 2, where a whole set of possible solutions may be obtained for each given b-value of the cloud. Two solutions seem to be possible, one around $b = 10$ km s^{-1} and another one around $b = 1.0$ km s^{-1}. The smaller b-value corresponds to an unrealistically high column density [N(D I) $\sim 3 \times 10^{19}$, or more than 10% of N(H)] and, in addition, is inconsistent with the relative weakness of D I–Lγ.

The $b = 10$ km s^{-1} solution corresponds to $N(\mathrm{D}) = 1.5 \times 10^{15}$ atoms cm^{-2} (deuterium column density) with a radial velocity of the order of 15 km s^{-1}. The

TABLE 1

INTERSTELLAR LINES AFFECTING D/H MEASUREMENTS*

Sp	λ	f
Lε		
O I	936.630†	...
(16,0)P(3)‡	936.859	3.06(−3)§
(17,0)P(5)	937.475	2.64(−3)
D I	937.548	7.80(−3)
(4,0)P(4)	937.553	6.40(−3)
H I	937.803	7.80(−3)
O I	937.841†	...
(15,0)R(0)	938.468	8.73(−3)
(16,0)R(4)	938.876	3.96(−3)
(18,0)R(7)	938.876	2.51(−3)
Lδ		
(15,0)P(4)	947.887	3.84(−3)
(17,0)P(7)	948.380	2.68(−3)
(3,0)R(3)	948.418	1.95(−2)
(14,0)R(2)	948.472	6.32(−3)
(3,0)Q(2)	948.618	2.73(−2)
O I	948.687†	...
(14,0)P(2)	949.355	4.21(−3):
D I	949.485	1.39(−2)
(3,0)P(2)	949.612	5.45(−3):
H I	949.743	1.39(−2)
(16,0)P(6)	949.845	3.25(−3)
(15,0)R(5)	950.102	4.70(−3)
(3,0)R(4)	950.316	1.82(−2)
(3,0)Q(3)	950.401	2.73(−2)
P IV	950.662	1.71(0)
(14,0)R(3)	950.820	6.00(−3)
O I	950.885†	...
N I	951.08†	...
N I	951.35†	...
Lγ		
(2,0)P(3)	970.560	9.92(−3)
(12,0)R(4)	970.835	8.29(−3)
Lγ		
(13,0)R(6)	970.994	6.70(−3)
(2,0)R(5)	971.073	2.21(−2)
(2,0)Q(4)	971.386	3.47(−2)
(14,0)P(7)	971.469	4.80(−3)
O I	971.738†	...
(11,0)R(0)	971.984	1.76(−2)
D I	972.272	2.90(−2)
F I	972.401†	...
H I	972.537	2.90(−2)
(12,0)P(4)	972.625	6.62(−3):
(11,0)R(1)	972.625	1.18(−2)
Cl IV	973.212	4.41(−2)
(11,0)P(1)	973.348	5.87(−3)
(2,0)P(4)	973.450	1.15(−2):
(13,0)P(6)	973.828	5.73(−3)
F I	973.895†	...
(11,0)R(2)	974.156	1.06(−2)
(2,0)Q(5)	974.286	3.46(−2)
Lβ		
(7,0)P(4)	1023.443	1.18(−2)
(8,0)P(6)	1022.563	1.14(−2)
(6,0)R(0)	1024.364	2.71(−2)
(8,0)R(7)	1024.980	1.31(−2)
(6,0)R(1)	1024.986	1.80(−2)
(7,0)R(5)	1024.991	1.44(−2)
D I	1025.443	7.91(−2)
H I	1025.722	7.91(−2)
O I	1025.762	7.3 (−2)
(6,0)P(1)	1025.932	9.00(−3)
Mg II	1025.968	1.48(−3)
Mg II	1026.113	7.40(−4)
(6,0)R(2)	1026.532	1.62(−2)
(7,0)P(5)	1028.255	1.20(−2)
(6,0)P(2)	1028.103	1.08(−2)
(6,0)R(3)	1028.986	1.54(−2)

* Data for H_2 from Morton and Dinerstein 1976. Atomic data from Morton and Smith 1973, or as noted in last footnote.

† Striganov and Sventitskii 1968.

‡ All such notation applied to the molecule H_2. For v'', the vibrational number of the upper electronic level, >5, the features are in the Lyman bands. Otherwise they are in Werner bands.

§ Notation to be read 3.06×10^{-3}.

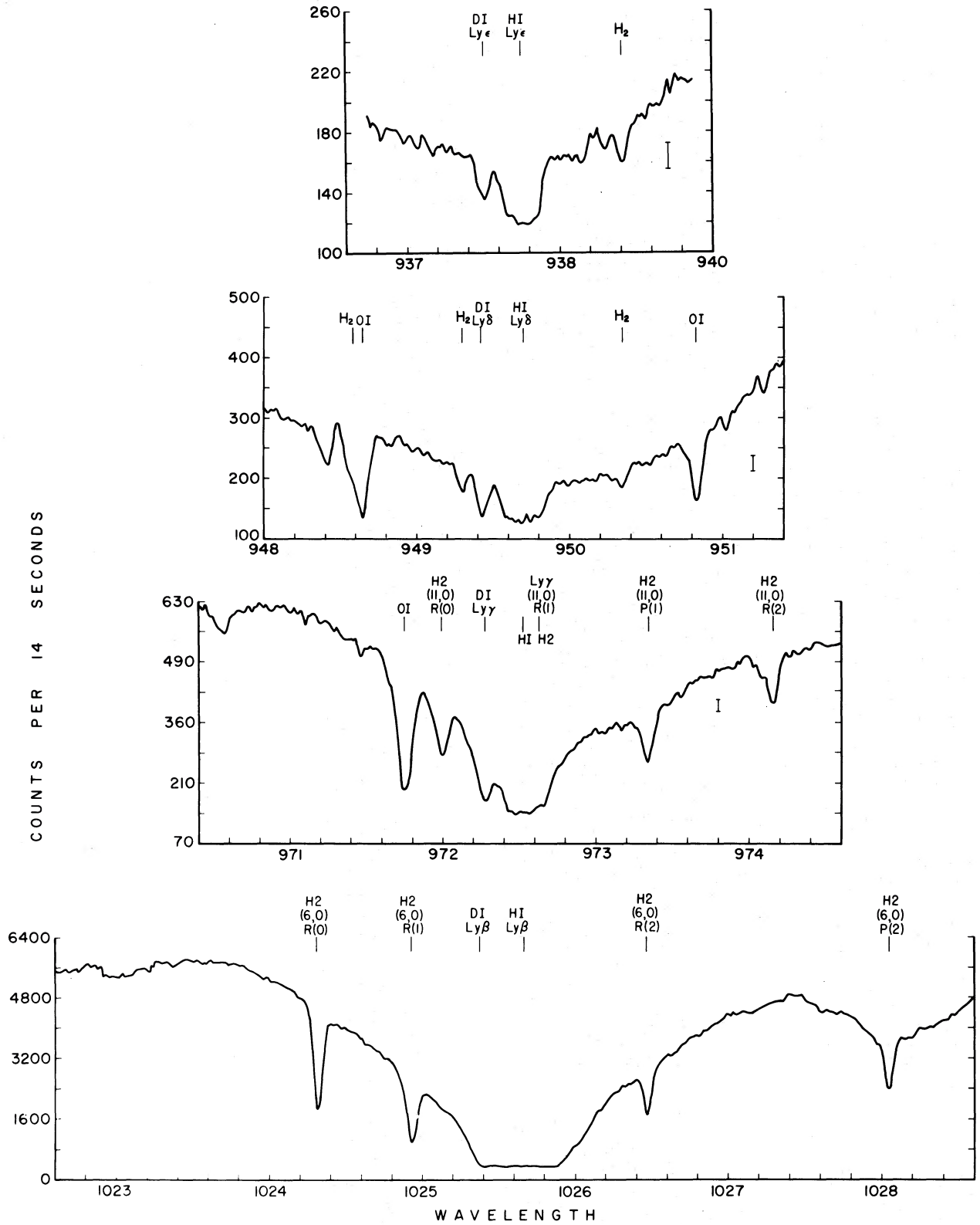

FIG. 1.—Averages of all scans in γ Cas (not monitored, as the data used in curve fitting were). The stellar Lyman lines are evident as broad absorption features. Theoretical $\pm 2\,\sigma$ error bars appear on the right for the top three graphs. Detected features are labelled.

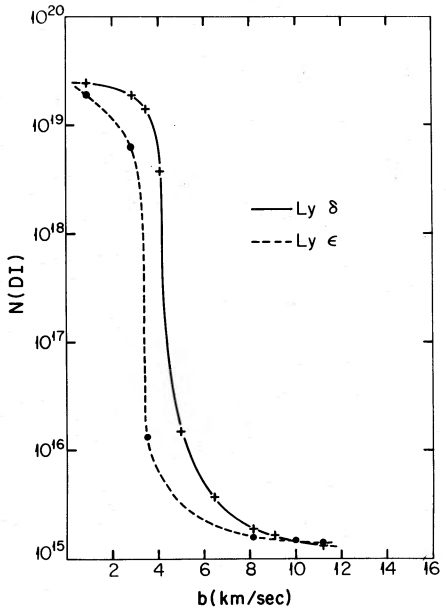

FIG. 2.—Solutions in the (b, N)-plane for Lδ and Lϵ in γ Cas. Acceptable solutions are the points of intersection.

velocity scale is discussed below. The b value of 10 km s^{-1} may represent a single cloud at 12,000 K, or a blend of cooler clouds spread out in velocity space to yield this effective b value. In Figure 3 are presented the fits of a solution where the corresponding hydrogen absorption features for the Lβ, Lγ, Lδ, and Lϵ lines are evaluated assuming the hydrogen is at the same temperature (b = 14 km s^{-1}) as that of deuterium with no turbulent motions. The agreement is excellent and shows that to the deuterium cloud corresponds a hydrogen cloud having the same parameters, radial velocity and temperature, with a column density of 1.0×10^{20} atoms cm^{-2}. Tests were performed to evaluate the sensitivity of the profile fits to changes in the parameters, such as background level and instrumental profile. It was found that changing the background by $\pm\sigma$ (rms deviation, as evaluated at the bottom of the saturated H I features), or changing the instrumental profile from 0.04 Å to 0.05 Å, does not seriously alter ($\pm 5\%$) the hydrogen column density due to the large saturated lines involved in the calculation; and the deuterium column density may be different by $\pm 20\%$, which in consequence represents approximately the error in the deuterium abundance evaluated under the assumption that the b-values are thermal in origin.

We have also attempted a solution where the internal motions of the assumed single cloud are purely turbulent motion ($b_H = b_D$). Fits for deuterium and hydrogen ($b_H = b_D$) are shown for differing values of N_H in Figures 4 and 5. The larger column densities are needed to replace the effect of the large value for b_H previously used to explain the wide line cores. The fits are not as good as those in Figure 3. In addition, the derived continuum (actually the stellar hydrogen line) is too high for Lγ (as well as for Lβ), assuming that the stellar lines should become deeper and deeper with increasing oscillator strength. The hydrogen column density should not be regarded as finally determined until the stellar and interstellar profiles can be simultaneously understood. However, we regard the quoted value [$N(H) = 1 \times 10^{20}$ cm^{-2}] to be accurate to $\pm 30\%$. We note that for a column density near 1×10^{20} cm^{-2} for H I and a high b-value for hydrogen, Lδ and Lϵ equivalent widths are quite sensitive to $b(W \alpha b)$, but insensitive to N(H I). The Lγ line is sensitive to b in the core and to N(H I) in the wings. The Lβ line is sensitive only to N(H I); but in the case where the behavior of the stellar background is not known (i.e., not quantitatively determined) the uncertainty in N(H I) derived only from Lβ can be large. Because of this primary dependence of Lϵ and Lγ on b, a comparison of the fits to these features in Figure 3 (b_H = 14 km s^{-1}) with those in Figures 4 and 5 (b_H = 10 km s^{-1}), shows that the value of b_H cannot be in error by more than 1.5 km s^{-1}. The value of b_D is known to similar accuracy. While the possibility that $b_H = b_D$ can therefore be ruled out, a combination of turbulence and thermal broadening could also explain the observations. For instance, assuming the effective b-value is a quadratic sum of turbulent and thermal values, then $T > 8000$ K, $b_{turb} < 6$ km s^{-1} are values consistent with the present data. The fact that $b_H > b_D$ could possibly be explained as being caused by high velocity hydrogen gas with $N_H < 10^{18}$ (so D I–Lβ is not detectable). Such gas would have to be symmetrically distributed about the main gas velocity to preserve the fact that the same values for central velocity fit the deuterium and hydrogen absorption features.

In Table 2 are presented the different observed and evaluated parameters representing the deuterium and hydrogen cloud. The velocity shifts (with respect to the star) as tabulated are strongly affected by the temperature of the spectrometer grating, for reasons not entirely understood (see Spitzer and Morton 1976). Unfortunately, the observations of γ Cas were broken up into two observing sessions, so that a large temperature transient occurred during the observations of Lγ. By measuring the velocities of individual lines on individual scans and plotting these versus the grating temperature (recorded at least once every 3 hours), an empirical relation for these particular observations shows a shift of 4.5 km s^{-1} K^{-1}, in the sense that a warming of the spectrometer causes the feature to have a more negative shift. According to Spitzer and Morton, velocities measured at a grating temperature of $-6.5°$ C ($-8.5°$ C at the front end of the spectrometer, as referred to in that paper) are in error by -16 km s^{-1}, if interstellar H_2 and Na I components are to appear at the same velocity. The correct velocity for the H I gas is therefore $+0.5$ km s^{-1} with respect to the star. For $v_* = -6.8$ km s^{-1}, $v_\odot = -6.3$ km s^{-1} and $v_\odot - v_{LSR} = -0.4$ km s^{-1}, where $v_\odot$ is the heliocentric velocity of the gas and v_{LSR} is the apparent velocity of gas

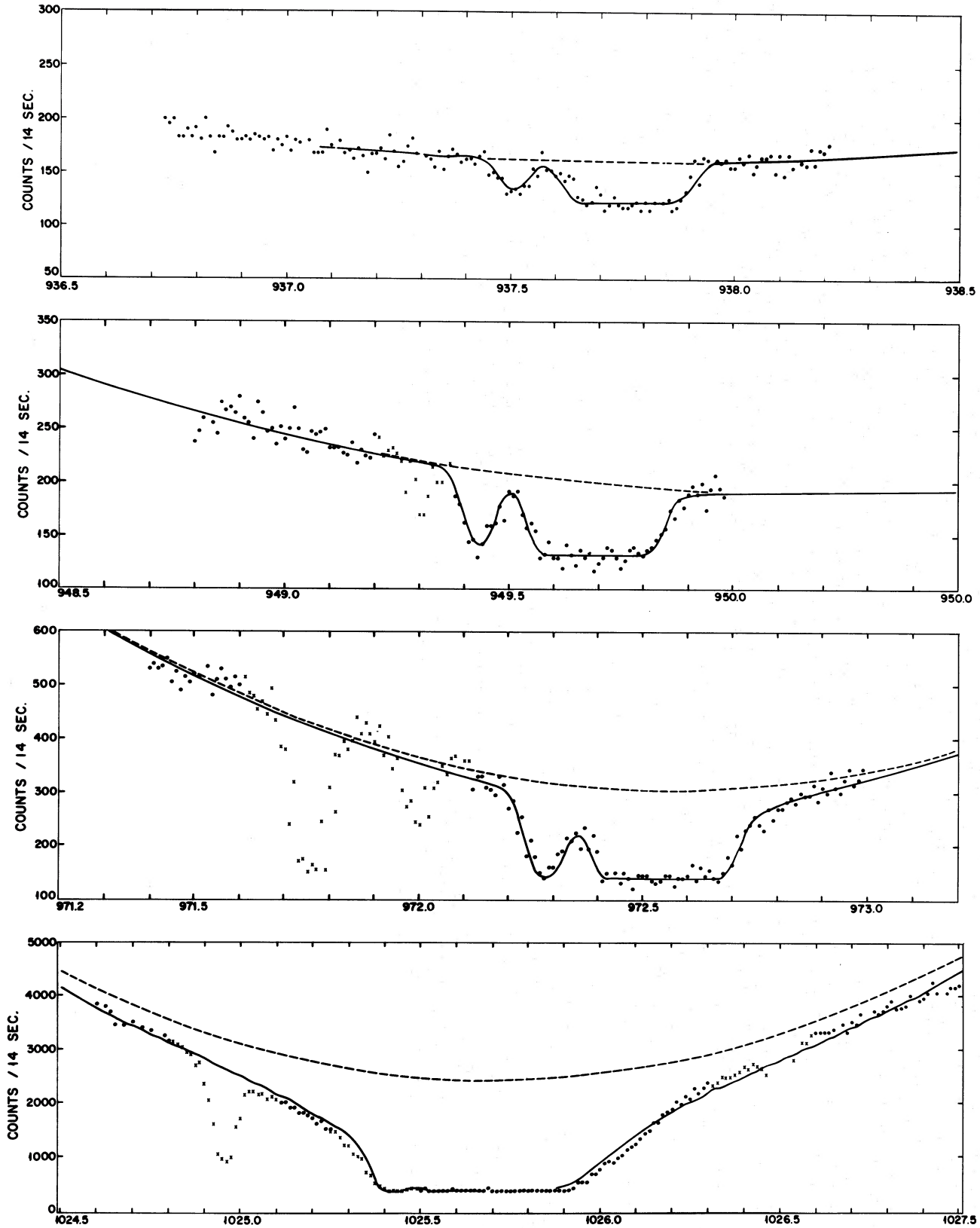

FIG. 3.—Final solutions for Lϵ, Lδ, Lγ, and Lβ in γ Cas. *Solid lines*, theoretical curves, convoluted with the instrumental profile, the parameters for which represent a least squares solution to the solid points. *Crosses*, points not included in the fit, as they obviously arise from absorption by species other than D I or H I. *Dashed lines*, the continua derived in the least squares fitting procedure (see text). The parameters for all four lines are close to $b_D = 10$ km s^{-1}, $b_H = 14$ km s^{-1}, N(D I) $= 1.5 \times 10^{15}$ cm^{-2}, N(H I) $= 1.0 \times 10^{20}$ cm^{-2}. Only a single component is necessary to fit the data.

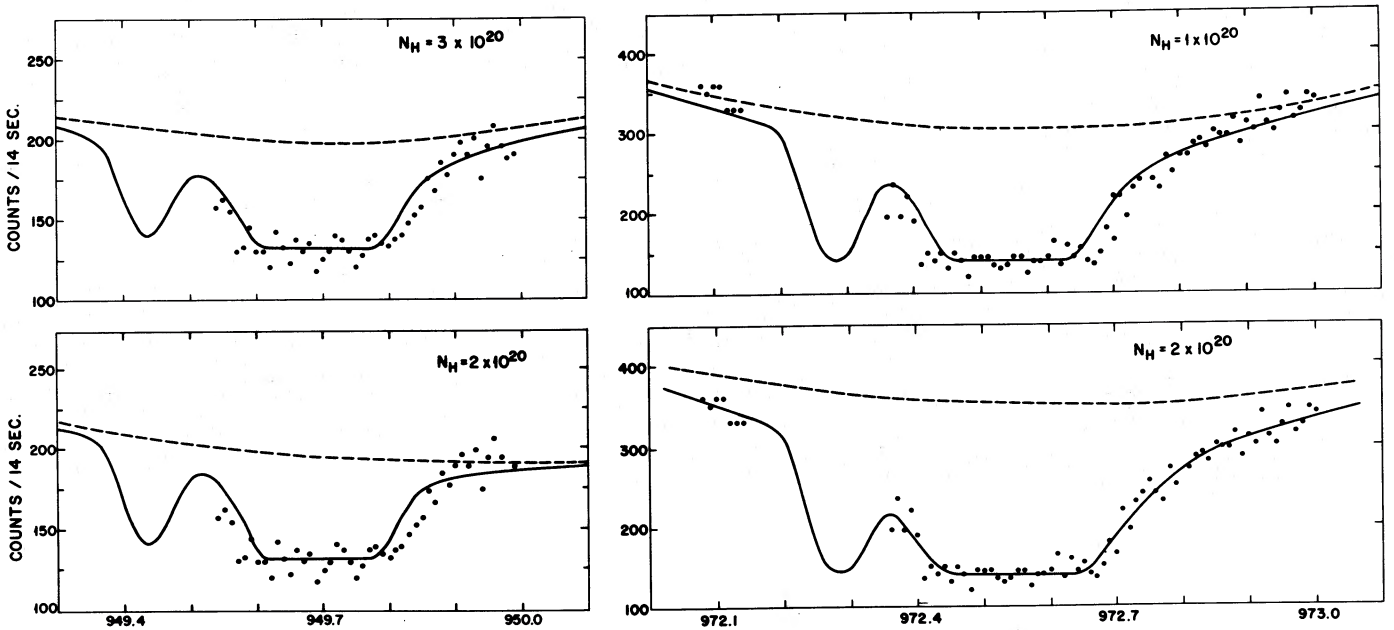

FIG. 4.—Attempts to fit (*left*) Lδ and (*right*) Lγ with $b_H = b_D$, and various H I column densities. Note that raising the H I column density also raises the underlying continuum, which is not consistent with the stellar Lyman lines becoming stronger with increasing f.

TABLE 2

THE γ CASSIOPEIAE LINE OF SIGHT

Parameter	Lβ	Lγ	Lδ	Lε
W_λ^H	1.14 Å	0.52 Å	0.37 Å	0.28 Å
W_λ^D	0.13 Å	0.10 Å	0.07 Å	0.05 Å
N^H	1.0×10^{20}	1.1×10^{20}	0.9×10^{20}	*
N^D	*	1.2×10^{15}	1.8×10^{15}	*
b^H (km s^{-1})	*	14	14	14
v_c (km s^{-1})	−7	+2.5	−16	−14
$T_{grating}$†	−4.8° C	−11 to −6° C	−6 to −6.5° C	−6.5° C

* No entry means the line is not sensitive to the parameter; however, in all cases the value derived from other lines is consistent.

† Princeton telemetry data for the thermocouple at the back of the spectrometer, about 18″ from the grating. The measurement is accurate to ±0.5 K.

stationary in the local standard of rest, due to the solar motion in this rest frame.

We find $N(\text{D I})/N(\text{H I}) = 1.5 \times 10^{-5} \pm 30\%$, in good agreement with previous observations (Papers I, II). Furthermore, the velocity distribution of the hydrogen and deuterium atoms simulates that of a warm cloud ($T \sim 12{,}000$ K, though $T > 8000$ K, $b_{turb} < 6$ km s^{-1} is consistent with the data). The half-width of the Na I line would be expected to be $1.7 \times b = 5.1$ km s^{-1} if the line widths are thermal, in good agreement with the line width of 6.5 km s^{-1} shown by Hobbs (1976), if the Na I feature is due to the same neutral gas producing H I and D I. Hobbs shows a heliocentric velocity of −4.5 km s^{-1}, about 2 km s^{-1} different from our value of −6.3 km s^{-1}. The Na I feature appears to be asymmetric, indicating multiple components. The *Copernicus* velocity scale could certainly be in error by 2 km s^{-1}. Since H I may exist in the absence of detectable Na I, the Na I data, while consistent with our analysis of the line of sight, is not conclusive evidence in favor of it.

The question now is to try to evaluate whether any solution is possible with more than one absorbing cloud separated by less than 8 km s^{-1} corresponding to the spectral resolution of the Princeton instrument.

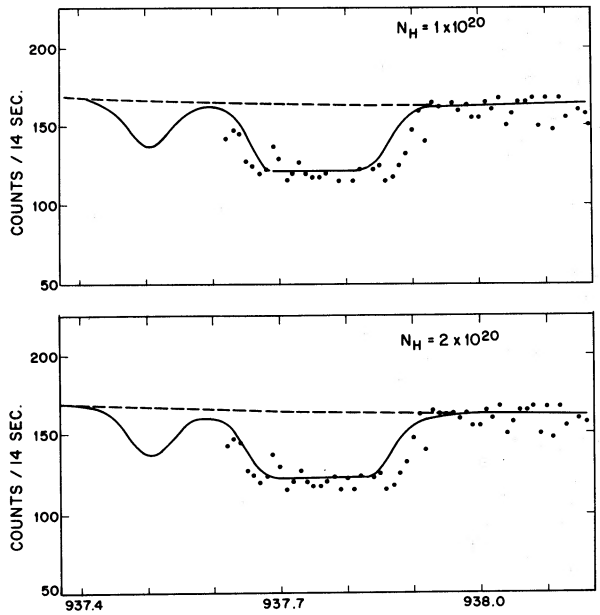

FIG. 5.—Same as Fig. 4, for Lε. Note that even for $N(\text{H I}) = 2 \times 10^{20}$ cm^{-2}, the theoretical profile is too narrow, implying $b_H > b_D$.

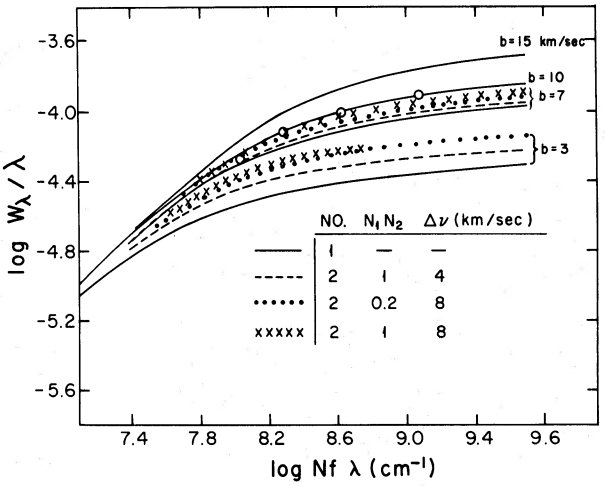

FIG. 6.—Theoretical Gaussian curves of growth for single and double (blended) components. The legend shows for the various kinds of curves the number of components involved, the ratio of column densities in the two components, and the separation in velocity between the two components. For two-component curves, the b-values of the two components are equal. Log W_λ/λ is the total width of the resulting feature and log $Nf\lambda$ includes the column density in both components. The open circles are for the derived equivalent widths and column densities of D I in γ Cas. The existence of multiple components with large b does not change the derived value N(D I) very much, as shown by the curves. The components with high b could be masking a narrow component with low b, but higher resolution is needed to see the effect if present. The presence of such a narrow component would force $N(\text{D I})/N(\text{H I})$ in the high b component to be larger than that derived, since N(H I) in any case is known independent of multiple components.

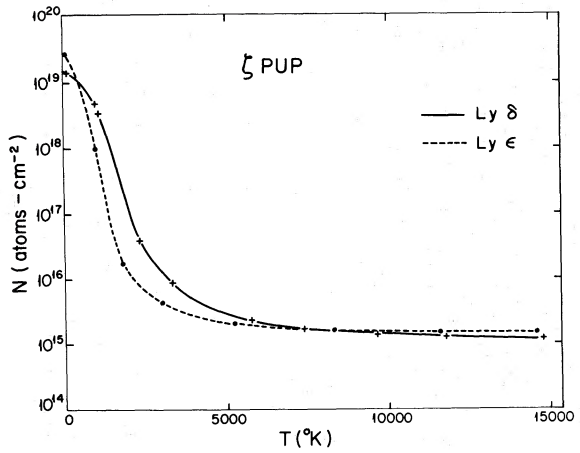

FIG. 7.—Solutions in the (T, N)-plane for Lδ and Lϵ in ζ Pup. The Gaussian analysis used $kT = 1/2\ mb^2$. The resulting T probably reflects turbulent motion or multiple component structure rather than kinetic temperature.

Figure 6, representing a curve of growth for one or two components of an equal b-value, shows that for a given absorption feature (a given W_λ value) the sum of column densities for two components is equal to less than the corresponding one-component column density. The difference may be particularly important for W_λ values corresponding to the plateau level.

We also show, in Figure 6, the derived equivalent widths corresponding to the computer fits shown in Figure 2. These show that in fact the deuterium lines agree with the expected behavior of lines with very large b near the linear portion. Since there is no evidence of incipient resolution of other components with $\Delta v > 8$ km s^{-1}, and since multiple components with smaller separation would yield a curve of growth similar to that observed, the deuterium column density cannot be much in error. However, the component structure could be more complex than assumed here, and observations at higher resolution would be highly desirable. The value N(D)/N(H) for the entire line of sight (1.5×10^{-5}) agrees with the average value for four stars given in Paper II. Components hidden in the present data could individually have higher or lower values. There is no evidence for this, and in fact the good agreement of the D I and H I profiles with the same temperature argues against there being separate velocity components of comparable importance in H I column density.

b) ζ *Puppis*

For ζ Pup, the spectral intervals scanned are much smaller than in the case of γ Cas, to give a larger number of observations in the narrow regions where the deuterium lines are located. These profiles appeared to be very clean and seem to contain much information.

The same procedure as for the γ Cas case was applied here, and on Figure 7 are presented the one-cloud solutions obtained for the Lδ and Lϵ deuterium absorption lines. Here again two types of solutions seem to be possible: a high b-value, low-N solution, and a low b-value, high-N solution. Again the large N solution is rejected due to the high deuterium column density obtained. Consistency with hydrogen is then checked here only with the hydrogen Lγ absorption line due to the lack of data on the two other weaker hydrogen lines. As noted earlier, Lδ and Lϵ are mainly sensitive to the b-value, not to N(H I).

Again we may check the solution under two different assumptions: same temperature or same b-value for the corresponding hydrogen cloud. Figure 8*a* shows the result of assuming a single cloud of hydrogen to go with the deuterium. From the position of the longward side of the core, b(H) > b(D) gives an unacceptable solution, so, unlike the previously studied case of γ Cas, we find $b_D \sim b_H$, implying that the velocity distribution is dominated by several cold components spread out in velocity space, but overlapping, or by turbulence in a single region. All attempts to find a solution with $b_H > b_D$ leaving the continuum as a free parameter failed. The continuum is sloping, due to the P Cygni profile of C III (977 Å) (Morton 1976), but it is smooth and well defined outside the region included in our own scans.

After several iterations it was found that another deuterium component, about −10 km s^{-1} from the main component, and with a similar b-value fits the deuterium data for Lϵ, Lδ, and Lγ. The corresponding hydrogen component is in fact needed to explain the extra absorption in the Lγ H I line of Figure 8. We note that failure to add this second component leaves one with the untenable situation of a single cloud with different velocities for D I and H I, as is evident from the theoretical-versus-observed profile in Figure 8*a*. The simplest solution derives if the second component does have a large b-value for H I, to fit the core of Lγ, Lδ, and Lϵ. Finally, another component, shifted by +6 to +16 km s^{-1} with respect to the main component of D I is necessary to fit the region between the two D I and the two H I components. It seems unlikely that this last component is D I, as H I gas with such a high velocity would not fit into the observed profile of H I, unless perhaps N(D I)/N(H I) were larger than 10^{-3}. Alternatively, the needed absorption could be H I gas at a velocity near −70 km s^{-1}. That the component is not some species other than H I or D I is shown by the fact that it is also required to fit profiles of Lγ, Lδ, and Lϵ.

The final fits for Lγ, Lδ, and Lϵ are shown in Figures 8*b*, 8*d*, and 9, respectively. The parameters for these fits are listed in Table 3. Figure 8*c* shows the effect of introducing a 3 km s^{-1} shift into the data, thus forcing the addition of another component at more negative velocities, and requiring one to move the uncertain component between D I and H I to longer wavelengths. The effect on the total column density of H I or D I is minimal. However, higher resolution would clearly be useful in allowing one to

TABLE 3

THE ζ PUPPIS LINE OF SIGHT

Parameter	Lβ	Lγ	Lδ	Lε
W_λ^H (Å)	1.23	0.52	0.35	0.31
W_λ^D (Å)	?	0.11	0.09	0.07
N^H1*	...	6×10^{18}	...	...
N^D1	2.3×10^{14}	1.3×10^{14}	1.3×10^{14}	...
b^H1 (km s^{-1})	...	16	16	16
v_c1 (km s^{-1})	...	+34	+33	+35
N^H2	0.8–0.6 $\times 10^{20}$	0.85×10^{20}	...	...
N^D2	1.8×10^{15}	1.8×10^{15}	1.76×10^{15}	1.76×10^{15}
b^H2 (km s^{-1})	...	7	7	7
v_c^2 (km s^{-1})	+30 to +43†	+43	+42	+44
N^U‡	...	2.7×10^{14}	1.4×10^{14}	1.5×10^{14}
v^U (km s^{-1})	...	−30	−30 to −12	−20
$b^H U$ (km s^{-1})	...	11	...	...
$T_{grating}$§ (°C)	−11	−11	−11	−11

* Column densities (cm^{-2}); b and v in km s^{-1}.

† See discussion in text. If $v = +43$ km s^{-1}, as would be the case based on Lε, γ, and δ, we find $N(D1) > 2 \times 10^{15}$, inconsistent with Lγ and Lδ. Either the velocity scale changed for some unknown reason between Lβ and Lγ scans, or some unidentified feature is absorbing shortward of D1.

‡ Extra absorption probably due to H I at high negative velocity. For D I, the velocities are given in Figs. 8 and 9.

§ ±1 K range in temperature observed.

assign ratio $N(D\,I)/N(H\,I)$ to very localized regions of space instead of relying on integrated values over long lines of sight, particularly since the results of any local deuterium production mechanisms are more likely to be apparent in low-column-density filaments than in a mean value for a large region of space.

We now try to verify the hydrogen column density with the observed Lβ profile. Bohlin (1975) gives $N(H) = 0.97 \times 10^{20}$. We show in Figure 10 (top) a profile of Lβ, assuming this column density. As is noted in the figure legend, the velocity of the main component of the gas, in the rest frame of the star, is +18 km s^{-1}, as opposed to +43 km s^{-1} for Lγ, Lδ, and Lε. Whereas velocity differences between Lβ, Lγ, Lδ, and Lε were noted earlier in γ Cas, these were well correlated with grating temperature, whereas the grating temperature for all four lines in ζ Pup was −11 K ± 0.5 K. (There was a break in the observations between Lγ and Lδ; but since the temperature was so similar, the wavelength scales should be consistent to ±5 km s^{-1}, as seems to be confirmed by our velocity analysis of Lγ and Lδ.) The average velocity of four nearby H_2 lines is +21 ± 4 km s^{-1} (av. dev.). According to Morton and Dinerstein (1976), the H_2 lines tend to be more negative than the neutral species such as Ar I and N I, by as much as −6 km s^{-1}. Since Spitzer and Morton (1976) have shown that the H_2 has a complex structure, more detailed information on the component structure is needed to use H_2 in deriving a velocity scale for H I and D I. We note, however, that with the velocity of H I Lβ required to obtain a column density of 1×10^{20} cm^{-2}, the negative velocity component of D I, which was near 1.5×10^{14} cm^{-2} from the fits to Lγ, Lδ, and Lε, is reduced to 1.3×10^{12} cm^{-2}. Furthermore, the derived continuum $[I(\lambda)e^{+\tau(\lambda)}$, where $I(\lambda)$ is the count rate at λ and $\tau(\lambda)$ is the optical depth in H I at λ] for $N(H\,I) = 1 \times 10^{20}$ cm^{-2}, is too high on the short-wavelength side and depressed on the long-wavelength side—the expected result if the assumed wavelength is too small (see Paper II). While a peculiar stellar profile underlying the interstellar absorption cannot be ruled out, there is no evidence for such behavior in the other Lyman lines. A search for Lβ emission from the surrounding nebula showed that contamination of the stellar spectrum by such a source is less than 0.1%. Lyman-β is seen in absorption against the P Cygni absorption profile of O VI 1031.945 Å (Morton 1976), and a search of the corresponding region of the O VI line at 1037.345 Å shows that the feature does not have apparent emission. By forcing Lβ to appear at the same velocity as the other lines (only the main H I component affects Lβ, which is primarily a damping profile), we find a column density $N(H\,I) = 6 \times 10^{19}$. This solution, however, raises $N(D\,I)$ in component D1 to 5×10^{15} cm^{-2}, quite inconsistent with values from Lγ and Lδ. We conclude that there was an unexpected change in the wavelength scale, or that some unexpected absorption is occurring. The O VI profile mentioned above may have broad excess absorption at Lβ (see

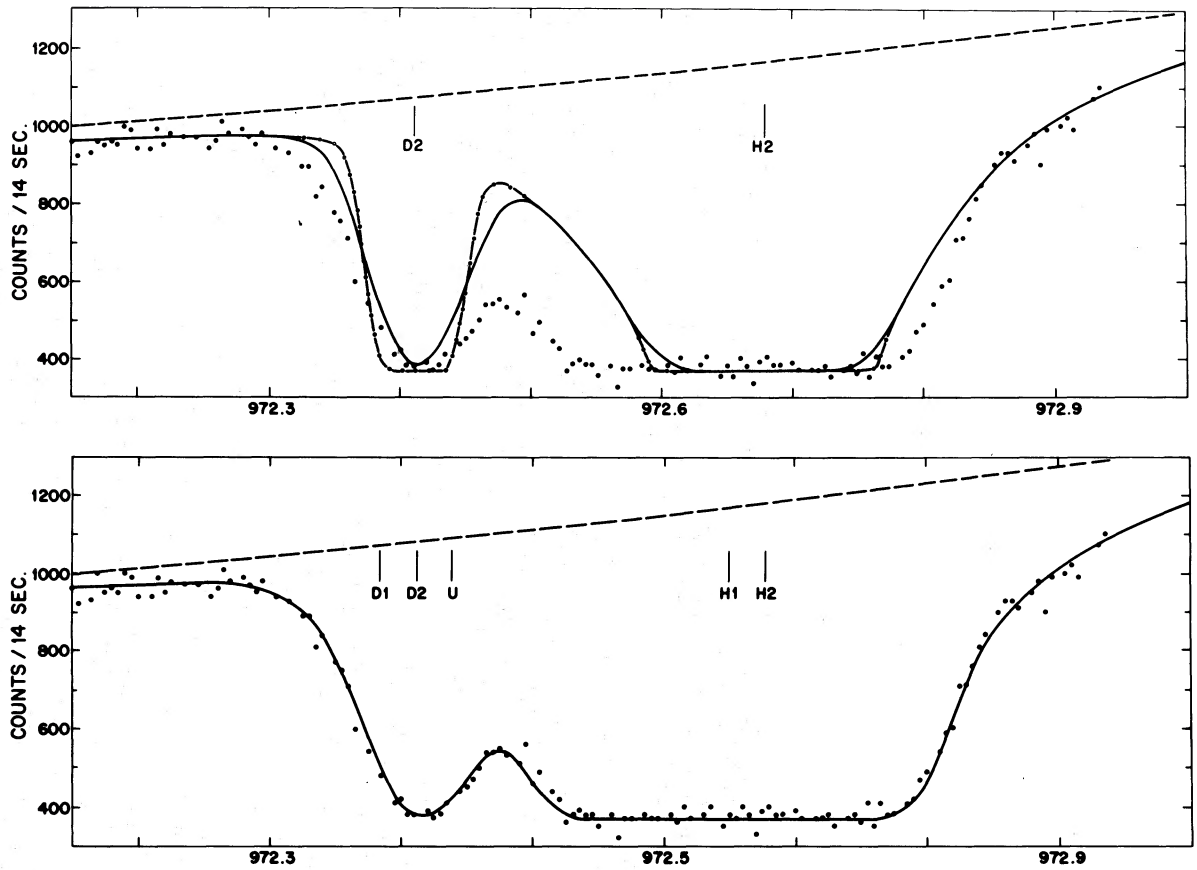

FIG. 8.—Trial solutions for N(D I) and N(H I) simultaneously in Lγ and Lδ. *Dashed lines*, the derived continuum; *solid lines*, the theoretical, convoluted profiles; *dot-dash lines*, the unconvoluted profiles. *Dots*, data points. Frame (*a*) is for one component at $+44$ km s^{-1} (stellar rest frame), $b_D = b_H = 7$ km s^{-1}, N(H I) $= 1 \times 10^{20}$ cm^{-2}, N(D I) $= 1.8 \times 10^{15}$ cm^{-2}. Frame (*b*) is for two main components: one at $+44$ km s^{-1}, $b = 8$ km s^{-1}, N(H I) $= 1 \times 10^{20}$ cm^{-2}, N(D I) $= 1.8 \times 10^{15}$; the other at $+35$ km s^{-1}, $b = 16$ km s^{-1}, N(H I) $= 6 \times 10^{18}$ cm^{-2}, N(D I) $= 1.3 \times 10^{14}$ cm^{-2}; a third component (U), with $N = 2.7 \times 10^{14}$, $b = 9$ km s^{-1} is D I at $+51$ km s^{-1} or more likely H I at -32 km s^{-1}. Frame (*c*) (Lδ) is for two components: one at $+45$ km s^{-1}, $b_H = b_D = 8$ km s^{-1}, N(H I) $= 1 \times 10^{20}$ cm^{-2}, N(D I) $= 1.76 \times 10^{15}$ cm^{-2}; the other at $+36$ km s^{-1}, $b_H = 16$ km s^{-1}, N(H I) $= 6 \times 10^{18}$ cm^{-2}, N(D I) $= 1.3 \times 10^{14}$; and the "U" component has $N = 9.1 \times 10^{13}$, $v = +69$ km s^{-1} (D I) or -14 km s^{-1} (H I). Frame (*d*) is similar to (*c*), except the two main components are 3 km s^{-1} shortward ($+42$, $+33$ km s^{-1}), while the "U" component is at $+51$ km s^{-1} (D I) or -32 km s^{-1} (H I) with $N = 1.4 \times 10^{14}$.

the profile of O VI in Morton 1976). The He II line at 1025.280 Å may also contaminate this region. Further work is needed on this problem. The value N(H I) seems certainly to lie within the bounds $8(+1, -2) \times 10^{19}$ cm^{-2}, based on minimizing the sum of the squares of the residuals at Lβ (see Fig. 10, bottom) and Lγ. This range cannot be made smaller, because a possible shift in the wavelength scale of Lβ relative to Lγ as large as 13 km s^{-1} cannot be ruled out.

The parameters for the one U (uncertain), two D I, and two H I components are listed in Table 3. We find formally, for component 1, N(D)/N(H) $= 2.2 \times 10^{-5}$ and for component 2, N(D)/N(H) $= 2.3(+0.7, -0.3) \times 10^{-5}$. The uncertainty of the former value is difficult to estimate, since, for the large b-value required, values of N(H I) based mainly on Lγ are somewhat uncertain for N(H I) $< 10^{19}$.

Component 2 may well be due to a combination of colder components, or to a velocity distribution of gas which is quite complex. In this case, the total deuterium column density of component 2 could be larger, though our observations of several lines do not allow too many saturated components to hide more material. For instance, we show in Figure 11 curves for N (sum of all subcomponents in cloud D2) versus T. The lines show solutions for 1 (*solid lines*) or 2 (*dashed lines*) subcomponents in D2 (the two subcomponents are assumed to have the same temperature, and are separated by Δv, which of course must vary as the temperature of the two components vary); the dashed lines show a possible solution for Lδ and Lϵ at N(D2) $= 4 \times 10^{16}$ cm^{-2}. The asterisk shows the overall column density for a three-subcomponent solution: two 300 K clouds and one 2000 K overlying them in velocity space, based on simultaneous fits in Lδ and Lϵ. Thus we cannot rule out the

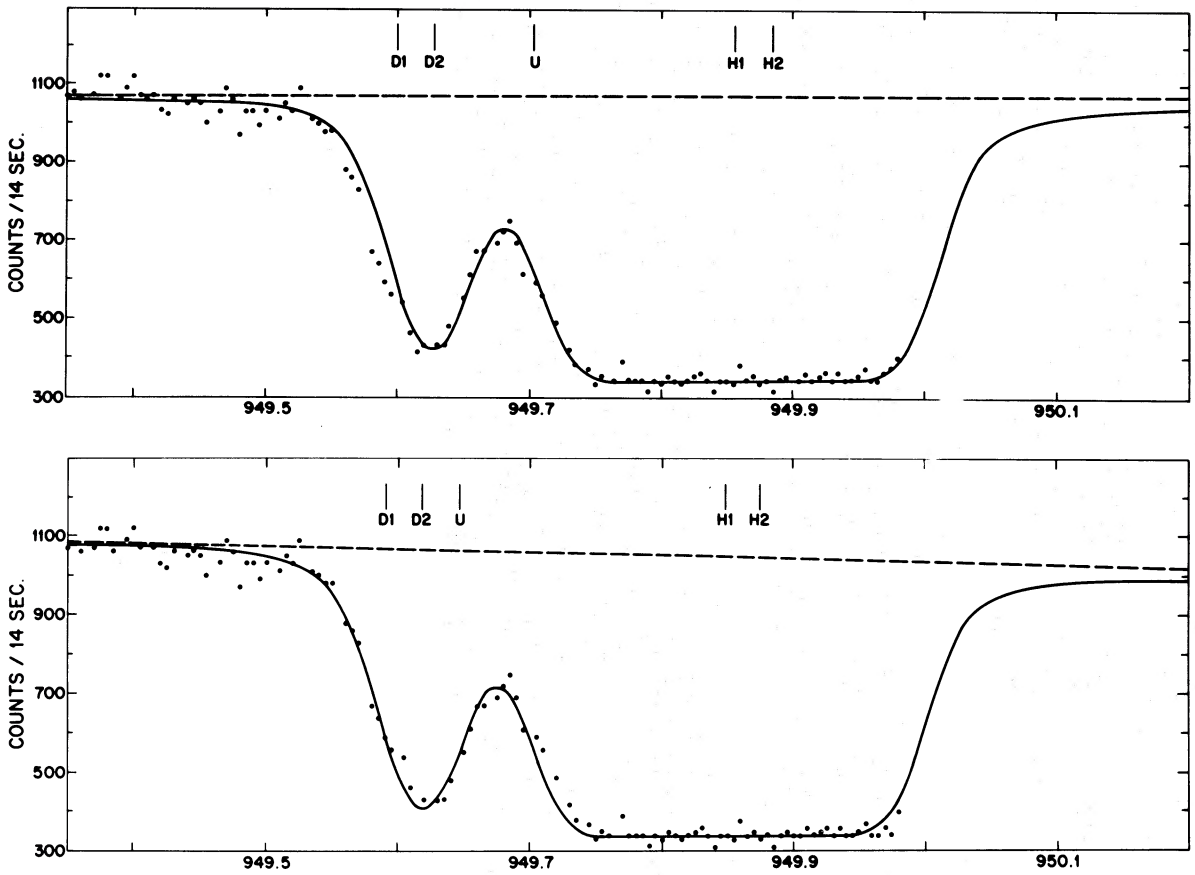

FIG. 8.—*Continued*

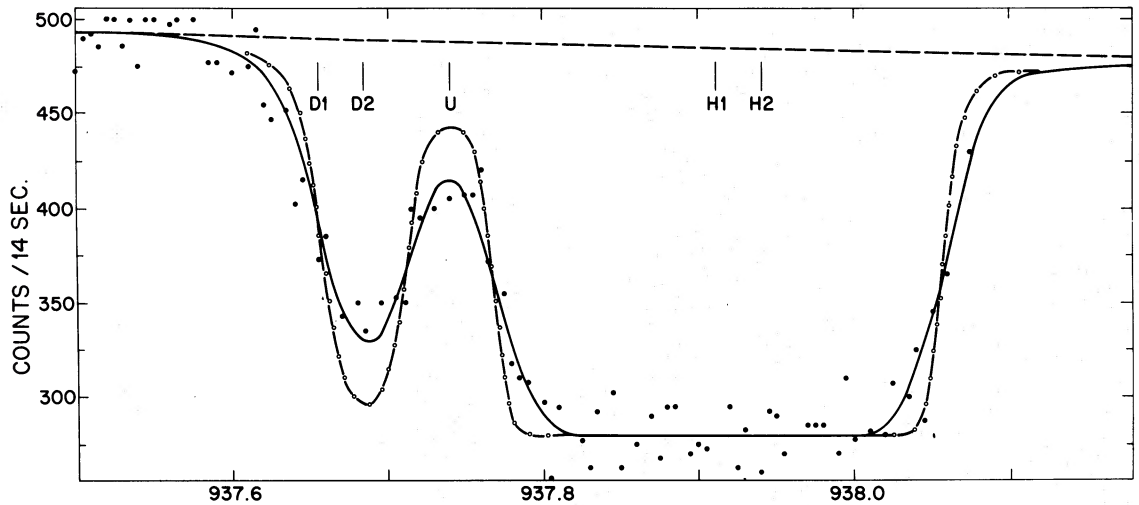

FIG. 9.—Final solution for Lε. The two main components have: $v = +44$ km s^{-1}, N(H I) $= 1.0 \times 10^{20}$ cm^{-2}, N(D I) $= 1.76 \times 10^{15}$ cm^{-2}, $b_B = b_H = 8$ km s^{-1}; $v = +35$ km s^{-1}, N(H I) $= 6 \times 10^{18}$ cm^{-2}, N(D I) $= 1.3 \times 10^{14}$ cm^{-2}, $b_B = b_H = 16$ km s^{-1}; a third ("U") component (see legend to Fig. 8) has $N = 1.47 \times 10^{14}$ cm^{-2}, $b = 9$ km s^{-1}, $v = +61$ km s^{-1} (D I) or $v = -21$ km s^{-1} (H I). The dash-dot line is the unconvoluted theoretical profile for these parameters; the solid line is the convoluted theoretical profile and the dashed line is the derived continuum. All data points were used in the fit.

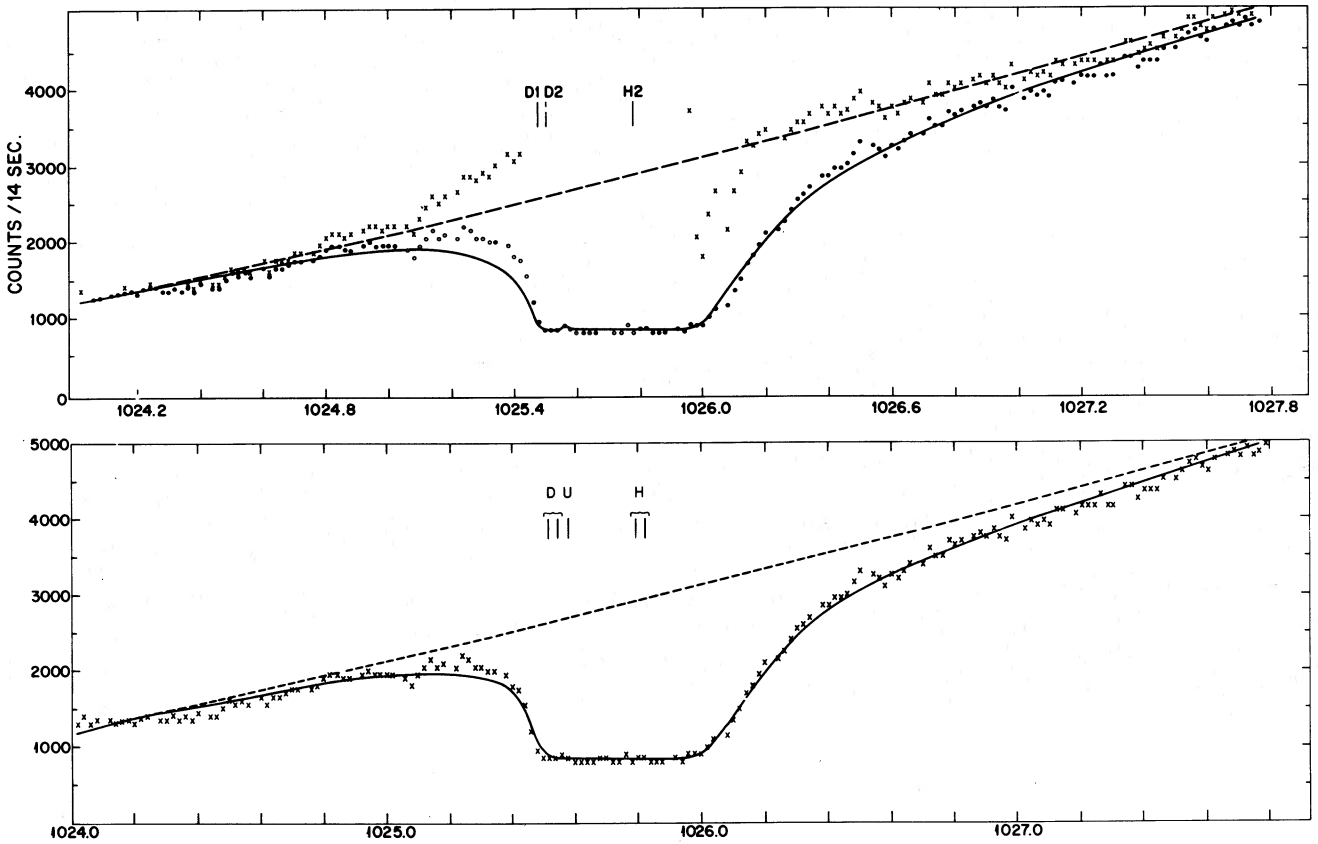

FIG. 10.—The fitted profile for Lβ assuming $N(\mathrm{H\ I}) = 10^{20}\ \mathrm{cm}^{-2}$ is shown at the top. *Dashed line*, the continuum derived; *solid line*, the theoretical profile (convoluted). The solid dots only were used in the fitting by least squares. Crosses show the result of multiplying individual count rate values by $e^{+\tau}$. Parameters implied by the fitting are, for the main component (2), $v = +18\ \mathrm{km\ s}^{-1}$, $N(\mathrm{H\ I}) = 1 \times 10^{20}\ \mathrm{cm}^{-2}$, $N(\mathrm{D\ I}) = 1.8 \times 10^{15}\ \mathrm{cm}^{-2}$, $b_{\mathrm{H}} = b_{\mathrm{D}} = 8\ \mathrm{km\ s}^{-1}$; for the secondary component (1), $v = +11\ \mathrm{km\ s}^{-1}$, $N(\mathrm{H\ I}) = 6 \times 10^{18}\ \mathrm{cm}^{-2}$, $N(\mathrm{D\ I}) = 1.3 \times 10^{12}\ \mathrm{cm}^{-2}$, $b_{\mathrm{H}} = b_{\mathrm{D}} = 16\ \mathrm{km\ s}^{-1}$. For Lβ, the sensitivity to $N(\mathrm{H\ I})$ and b for this latter component is not high. The column density $N(\mathrm{H\ I}) = 10^{20}$ appears to be too high, since $N(\mathrm{D\ I})$ in the secondary component is 100 times less than required for Lγ and Lδ, the velocity shift ($|v_1 - v_2|$) is too small, and the $e^{+\tau}$ solutions do not meet for the two wings. A shift to $+44\ \mathrm{km\ s}^{-1}$, with $N(\mathrm{H\ I}) = 6 \times 10^{19}$ better fits all the data (see text), but for the $N(\mathrm{D\ I})$ of the secondary component which is then more than 10 times too large (see Table 3). The bottom frame shows the best fitting profile (in a least squares sense). The solution represented differs from that for the top frame in that $N(\mathrm{H\ I}) = 0.8 \times 10^{20}$, $v = +30\ \mathrm{km\ s}^{-1}$ for component 2; $N(\mathrm{D\ I}) = 2.3 \times 10^{14}\ \mathrm{cm}^{-2}$, $v = +21\ \mathrm{km\ s}^{-1}$ for component 1; and $N = 2 \times 10^{14}\ \mathrm{cm}^{-2}$, $b = 12.8\ \mathrm{km\ s}^{-1}$, $v = -42\ \mathrm{km\ s}^{-1}$ for component "U" (not included in the solution in the top frame).

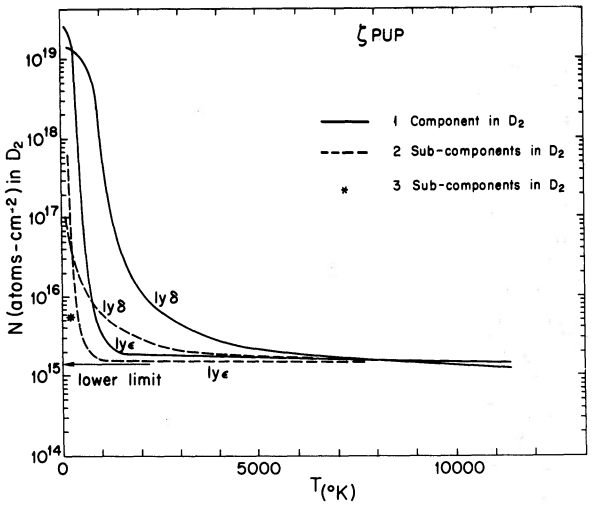

FIG. 11.—Solutions in the (N, T)-plane for Lδ and Lε, assuming multiple components. Solid lines are assuming components D1 and D2 (solution 2 in Fig. 12). Dashed lines are for D1 plus two subcomponents in D2 at the same temperature represented on the abscissa (solution 3 of Fig. 12). The asterisk is the point of intersection for Lδ and Lε curves computed assuming the presence of D1 and D2, with D2 divided among three subcomponents: two 300 K components to represent the sharp edges of the absorption feature and one 2000 K component to fill up the center with not too many atoms. The curves were defined by finding least squares solutions for N (the total column density of the D_2 deuterium component) for various values of the temperature in that main component.

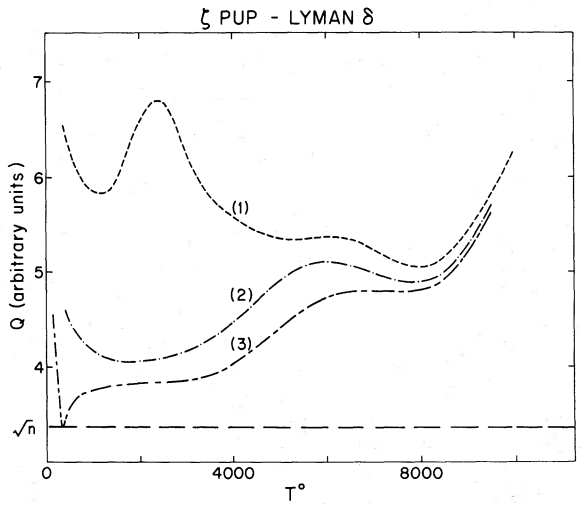

FIG. 12.—Q, the sum of the residuals of observed data points, as a function of the internal temperatures of the main deuterium components, for one, two, and three components. Solution 1 corresponds to 1 component only in the observed deuterium profile (Fig. 7). Solution 2 assumes two components, D1 and D2 (Fig. 8); the temperature of D2 is varied. Solution 3 corresponds to solutions including D1 and D2, but D2 is assumed to contain two subcomponents, separated by Δv (see text). The temperature in the two subcomponents of D2 (equal in the two) is varied. The line marked $\sqrt{n}$ is the locus of points which could represent the best possible fit at any given T due to statistical fluctuations in the data. Within D2, for $T =$ 300 K, $\Delta v = 6$ km s^{-1} (solution 3). This set of parameters provides the best formal fit to the data.

existence of fairly large column densities of deuterium in our component 2, but models can be formulated which do not require such large values.

In Figure 12 we show Q (sum of the square of the departures between the measurements and the calculations) versus the temperature of the main deuterium component. Solution 1 is from the fitting of the entire deuterium profile, corresponding to Figure 7. Solution 2 is from the fitting of two components (D1 and D2), with the temperature of D2 changing along the abscissa. Solution 3 is from the fit using D1, and two subcomponents in D2 separated by Δv, with varying but identical temperatures (*dashed lines* in Fig. 11). The lower Q-value for solution 3 essentially indicates that the D2 component needs sharp edges. The profile for solution 3 is shown in Figure 13. Shallower edges for the theoretical profile (*dash-dot line*) would worsen the fit of the data points with the solid line which shows the effects of the instrumental profile on the theoretical profile. Thus any attempt to model D2 in detail probably cannot include strong components that are warm and which would thus round off the edges. The asterisk in Figure 11 shows that we can lower the value of N in D2 by including one warm and two 300 K subcomponents. In all probability a more complex solution involving many very sharp slightly saturated components could be used to lower the derived column densities, down to the limit shown. Such a model is equivalent to claiming that the velocity distribution is square in shape. Such a distribution could be observed, for instance from a diverging stream of cold material crossing the line of sight, or by many clouds with Gaussian distribution slightly separated in velocity space. Higher resolution observations are clearly of interest for component D2. Profile analysis of other neutral species, such as N I, Ar I, and O I, would also be useful in confirming this rather peculiar velocity distribution. For these species spectral features can be found with a lower product of Nf, so that our components D1 and "U" would not complicate the analysis.

All velocities quoted for ζ Pup are in the rest frame of the star, which has a heliocentric velocity of -24 km s^{-1}. The velocity $v_{\rm LSR} = 18$ km s^{-1} for ζ Pup. Whereas our γ Cas value could be directly tied into the calibration temperature of Spitzer and Morton (1976), our ζ Pup data were taken at a lower temperature, so cold in fact that there is probably little systematic error in the velocity scale. However, since this cannot be definitely demonstrated, our absolute velocities are uncertain by ± 10 km s^{-1}. We find $v_{\odot 2} = +20$ km s^{-1}, $v_{\odot 1} = +11$ km s^{-1}, $v_{\odot u} = -50$ km s^{-1}; $v_{\odot 2} - v_{\rm LSR} = +2$ km s^{-1}, $v_{\odot 1} - v_{\rm LSR} = -7$ km s^{-1}, $v_{\odot u} - v_{\rm LSR} = -68$ km s^{-1}.

Wallerstein and Silk (1971) have noted the presence of high-velocity components of ionized calcium in the vicinity of the Puppis-Vela region. The presence of our component U and its probable identification with high-velocity H I implies that this line of sight is

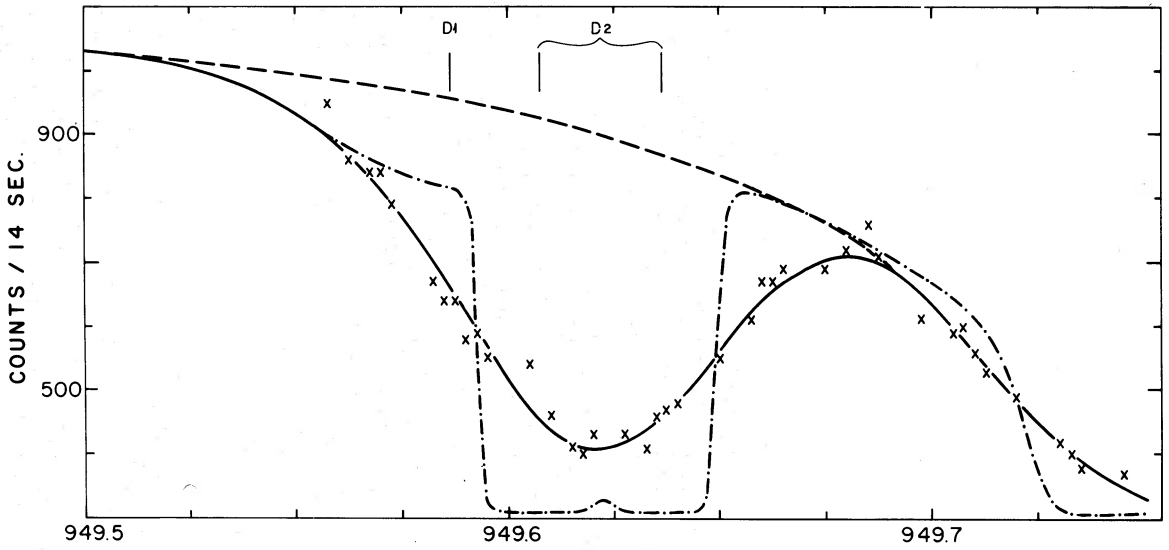

FIG. 13.—The best fit corresponding to the lowest Q-value over the deuterium Lδ (see Fig. 12, solution 3) within component D2: two cold subcomponents at $T = 300$ K, $\Delta v = 6$ km s^{-1}, each with N(D I) $\sim 1.7 \times 10^{16}$ cm^{-2} (see Fig. 11, solution with 2 subcomponents in D2).

likely very complex and that much structure is masked at our resolution.

V. CONCLUSIONS

The interstellar gas between the Sun and γ Cas is characterized by a ratio N(D I)/N(H I) of 1.5×10^{-5}, apparently mostly due to a component at high temperature. The gas between the Sun and ζ Pup appears to be distributed in a more complex manner. We find two components, separated by 10 km s^{-1}, differing in total H I column density by a factor of 10, though the ratio N(D I)/N(H I) may be comparable. One of these (component 2) is apparently complex. While we cannot rule out the possibility that all three components directly observed in spectra of γ Cas and ζ Pup have the same ratio N(D I)/N(H I) as that found in Paper II (1.5×10^{-5}), ζ Pup may well contain components enriched in D I. For both lines of sight, observations of other neutral species at higher resolution would add considerably to the conclusiveness of the results. Apart from models for the velocity distribution of the line of sight, the largest uncertainties are in the determinations of N(H I); further efforts to refine the quoted values are warranted.

Spitzer and Morton (1976) list two components in ζ Pup containing H_2, which are separated by 10 km s^{-1}. However, their detailed data show that the separation varies from one transition to another, perhaps another sign of the complexity of this line of sight. Because of uncertainties in the velocity scales at different observing orbits, we cannot be sure if our components 1 and 2 coincide with theirs. It is important to try to resolve the present uncertainty, as the determination of N(D I) in individual components could lead directly to the ratio $N(H_2)/N$(H I) in each component, allowing more meaningful densities for each gas cloud to be derived (Jura 1975).

This research was supported in part by contract NAS5–1810 to Princeton University from NASA. We wish to thank J. Wrigley for assistance in data compilation and handling. Three of us (A. V.-M., R. M. B., C. L.) would like to thank very much L. Spitzer, J. Rogerson, and the whole Princeton team on *Copernicus* for their cooperation. They are also indebted to P. Bruston and J. P. Delaboudiniere for their participation in the definition of their Guest Investigator Program, and to J. Audouze and J. Lequeux for fruitful discussions.

Numerical computations were completed on the CDC 7600 computer of CNES from the laboratory in Verrieres-le-Buisson (France).

REFERENCES

Anglin, J. D., Dietrich, W. F., and Simpson, J. A. 1973, *Ap. J.* (*Letters*), **186**, L41.
Audouze, J., and Tinsley, B. M. 1974, *Ap. J.*, **192**, 487.
Beer, R., and Taylor, F. W. 1973, *Ap. J.*, **179**, 309.
Black, D. C. 1972, *Geochim. Cosmochim. Acta*, **36**, 347.
Bohlin, R. C. 1975, *Ap. J.*, **200**, 402.
Cesarsky, D. A., Moffet, A. T., and Pasachoff, J. M. 1973, *Ap. J.* (*Letters*), **180**, L1.
Colgate, S. A. 1975, *Ap. J.*, **195**, 493.
Geiss, J., and Reeves, H. 1972, *Astr. Ap.*, **18**, 126.
Gomez-Gonzalez, J., and Lequeux, J. 1975, *Astr. Ap.*, **38**, 29.
Hobbs, L. M. 1969, *Ap. J.*, **157**, 135.
———. 1976, *Ap. J.*, **203**, 143.
Jura, M. 1975, *Ap. J.*, **197**, 575.
Kaper, H. G., Smits, D. W., Schwarz, U., Takakubo, K., and van Woerden, H. 1966, *B.A.N.*, **18**, 465.
Marschall, L. M., and Hobbs, L. M. 1972, *Ap. J.*, **173**, 43.
Morton, D. C. 1976, *Ap. J.*, **203**, 386.
Morton, D. C., and Dinerstein, H. 1976, *Ap. J.*, **204**, 1.
Morton, D. C., and Morton, W. A. 1972, *Ap. J.*, **174**, 237.

Morton, D. C., and Smith, W. H. 1973, *Ap. J. Suppl.*, **26**, 333.
Nachman, P., and Hobbs, L. M. 1973, *Ap. J.*, **182**, 481.
Ostriker, J. P., and Tinsley, B. M. 1975, *Ap. J.* (*Letters*), **201**, L51.
Pasachoff, J. M., and Cesarsky, D. A. 1974, *Ap. J.*, **193**, 65.
Quirk, W. J., and Tinsley, B. M. 1973, *Ap. J.*, **179**, 69.
Reeves, H., Audouze, J., Fowler, W. A., and Schramm, D. N. 1973, *Ap. J.*, **179**, 909.
Rogerson, J. B., Spitzer, L., Drake, J. F., Dressler, K., Jenkins, E. B., Morton, D. C., and York, D. G. 1973, *Ap. J.* (*Letters*), **181**, L97.
Rogerson, J. B., and York, D. G. 1973, *Ap. J.* (*Letters*), **186**, L95 (Paper I).
Spitzer, L., Drake, J. F., Jenkins, E. B., Morton, D. C., Rogerson, J. B., and York, D. G. 1973, *Ap. J.* (*Letters*), **181**, L116.
Spitzer, L., and Morton, W. A. 1976, *Ap. J.*, **204**, 731.
Striganov, A. R., and Sventitskii, N. S. 1968, *Tables of Spectral Lines of Neutral and Ionized Species* (New York: IFI/Plenum).
Talbot, R. J., and Arnett, W. D. 1973, *Ap. J.*, **186**, 51.
Trauger, J. T., Roesler, F. L., Carleton, N. P., and Traub, W. A. 1973, *Ap. J.* (*Letters*), **184**, L137.
Truran, J. W., and Cameron, A. G. W. 1971, *Ap. Space Sci.*, **14**, 179.
Wagoner, R. V. 1973, *Ap. J.*, **179**, 343.
Wilson, R. W., Penzias, A. A., and Jefferts, K. B. 1973, *Ap. J.* (*Letters*), **179**, L107.
Yahil, A., and Beaudet, G. 1976, *Ap. J.*, **206**, 26.
York, D. G., Drake, J. F., Jenkins, E. B., Morton, D. C., Rogerson, J. B., and Spitzer, L. 1973, *Ap. J.* (*Letters*), **182**, L1.
York, D. G., and Rogerson, J. B. 1976, *Ap. J.*, **203**, 378 (Paper II).

R. M. BONNET, C. LAURENT, and A. VIDAL-MADJAR: Laboratoire de Physique Stellaire et Planetaire, Centre National de la Recherche Scientifique, Verrieres-le-Buisson, France

DONALD G. YORK: Princeton University Observatory, Princeton, NJ 08540